Int. J. Heat Mass Transfer. Vol. 36, No. 4, pp. 899–906, 1993
Printed in Great Britain

0017-9310/93 $6.00 + 0.00

Improving effectiveness of pipe insulation by using radial baffles to suppress natural convection

F. C. LAI†

Department of Mechanical Engineering, Colorado State University, Fort Collins, CO 80523, U.S.A.

(*Received* 27 *November* 1991 *and in final form* 11 *May* 1992)

Abstract—In this paper, the feasibility of using radial baffles to improve the effectiveness of pipe insulation is investigated numerically. Three baffle designs have been considered, i.e. full baffles, partial inner baffles and partial outer baffles. These designs have been applied to the case of horizontal pipe insulation. Calculations have covered a range of Rayleigh numbers of practical interest (i.e. $50 \leqslant Ra \leqslant 500$). In addition, the relations between the heat loss and the baffle orientation angle is carefully examined for each pipe–baffle configuration. The results show that radial baffles are effective to suppress the natural convection that arises in a pipe insulation. The effectiveness increases with the baffle number. It has also shown that partial baffles work better than full baffles. At a high Rayleigh number ($Ra = 500$), the flow and temperature fields at some orientation angles become unstable. The averaged heat transfer, however, is still less when using baffles.

INTRODUCTION

IT IS WELL known that natural convection within insulation accounts for the major loss of useful energy. It has become one of the important considerations in process design to suppress this non-beneficial convective transport. For pipes, this can be achieved by several methods. For example, using eccentric insulation is one [1] and applying layers of insulation is another [2]. In this study, we numerically investigated the feasibility of using radial baffles to improve pipe insulation. The same technique has been used by others to suppress natural convection in air-filled annuli and proved to be very successful [3–6]. However, the previous studies [3–6] were limited to either a specific baffle geometry or a fixed baffle orientation.

In this study, three baffle designs have been considered, i.e. full baffles, partial inner baffles and partial outer baffles (Fig. 1). For each design, the orientation of the baffles was varied parametrically to reveal the complexity in flow patterns, temperature distribution and heat transfer. Results which include the Nusselt versus Rayleigh number relation in terms of the baffle size and location will be presented.

ANALYSIS

Most pipe insulation available today can be adequately modeled as a porous annulus (Fig. 1). For most applications, the inner cylinder is heated at a constant temperature T_i while the outer cylinder is maintained at the ambient temperature T_o ($T_i > T_o$).

The governing equations based on Darcy's law are given by

$$\frac{\partial v_r}{\partial r} + \frac{v_r}{r} + \frac{1}{r}\frac{\partial v_\theta}{\partial \theta} = 0 \tag{1}$$

$$v_r = -\frac{K}{\mu}\left(\frac{\partial p}{\partial r} + \rho g \sin\theta\right) \tag{2}$$

$$v_\theta = -\frac{K}{\mu}\left(\frac{1}{r}\frac{\partial p}{\partial \theta} + \rho g \cos\theta\right) \tag{3}$$

$$\sigma\frac{\partial T}{\partial t} + v_r\frac{\partial T}{\partial r} + \frac{v_\theta}{r}\frac{\partial T}{\partial \theta} = \alpha\left[\frac{1}{r}\frac{\partial}{\partial r}\left(r\frac{\partial T}{\partial r}\right) + \frac{1}{r^2}\frac{\partial^2 T}{\partial \theta^2}\right]. \tag{4}$$

The transient form of the energy equation is stated here for completeness. For the steady-state analysis, the time derivative term is set to zero. Having invoked the Boussinesq approximation, the governing equations can be non-dimensionalized to give

$$\frac{\partial V_\theta}{\partial R} + \frac{V_\theta}{R} - \frac{1}{R}\frac{\partial V_r}{\partial \theta} = Ra\left(\cos\theta\frac{\partial \Theta}{\partial R} - \frac{\sin\theta}{R}\frac{\partial \Theta}{\partial \theta}\right) \tag{5}$$

$$\frac{\partial \Theta}{\partial \tau} + V_r\frac{\partial \Theta}{\partial R} + \frac{V_\theta}{R}\frac{\partial \Theta}{\partial \theta} = \frac{1}{R}\frac{\partial}{\partial R}\left(R\frac{\partial \Theta}{\partial R}\right) + \frac{1}{R^2}\frac{\partial^2 \Theta}{\partial \theta^2} \tag{6}$$

with the boundary conditions given by

$$\Theta = 1/2, \quad V_r = 0, \quad \text{on the inner wall} \tag{7a}$$

$$\Theta = -1/2, \quad V_r = 0, \quad \text{on the outer wall.} \tag{7b}$$

As for the baffles, they are assumed to be very thin such that the angular temperature gradient is negligible. Thus, the appropriate boundary conditions

† Presently at: School of Aerospace and Mechanical Engineering, University of Oklahoma, Norman, OK 73019, U.S.A.

NOMENCLATURE

D	gap width, $r_o - r_i$
g	acceleration due to gravity
H	length of baffle
h	average heat transfer coefficient
K	permeability
k	effective thermal conductivity
N	number of baffles
Nu	average Nusselt number, hD/k
p	pressure
R	dimensionless radial distance, r/D
r	radial distance
Ra	Rayleigh number, $Kg\beta(T_i - T_o)D/\alpha\nu$
T	temperature
t	time
T_m	mean temperature, $(T_i + T_o)/2$
V_r	dimensionless velocity in the r-direction, $1/R(\partial\psi/\partial\theta)$
V_θ	dimensionless velocity in the θ-direction, $-\partial\psi/\partial R$
v_r	Darcy velocity in the r-direction, $\alpha V_r/D$
v_θ	Darcy velocity in the θ-direction, $\alpha V_\theta/D$
W	dimensionless thickness of baffle, w/D
w	thickness of baffle.

Greek letters

α	thermal diffusivity of porous medium
β	coefficient of thermal expansion, $(-1/\rho)(\partial\rho/\partial T)_p$
γ	orientation of the referenced baffle with respect to the vertical diameter
ε	porosity
Θ	dimensionless temperature, $(T - T_m)/(T_i - T_o)$
θ	angular coordinate
μ	dynamic viscosity
ν	kinematic viscosity
ρ	density of convective fluid
σ	heat capacity ratio of the saturated porous medium to that of the fluid, $[\varepsilon(\rho c)_f + (1-\varepsilon)(\rho c)_s]/(\rho c)_f$
τ	dimensionless time, $t/(\sigma D^2/\alpha)$
ψ	stream function.

Subscripts

b	baffle
cond	conduction mode
f	fluid phase
i	inner cylinder
m	mean value
o	outer cylinder
s	solid phase.

on the baffles are given by

$$V_\theta = 0 \tag{7c}$$

$$k_b W \frac{\partial^2 \Theta}{\partial R^2} = \frac{k}{R}\left(\left.\frac{\partial \Theta}{\partial \theta}\right|_1 - \left.\frac{\partial \Theta}{\partial \theta}\right|_2\right) \tag{7d}$$

where subscripts 1 and 2 refer to the two sides of the baffle. Equation (7d) has been derived by performing an energy balance for the baffle. This boundary condition has also been employed by Kwon *et al.* [4] in a similar study.

To solve the simultaneous equations defined above, a numerical model that was used to simulate the natural convection in a truncated circular sector of porous medium has been utilized [7]. The model uses the following coordinate transformation to map the computational domain onto a rectangular geometry to facilitate calculations.

$$x = \frac{\ln R - \ln R_i}{\ln R_o - \ln R_i} - \frac{1}{2}, \quad y = \frac{\theta - \theta_i}{\theta_o - \theta_i}. \tag{8}$$

Thus, the governing equations are transformed to

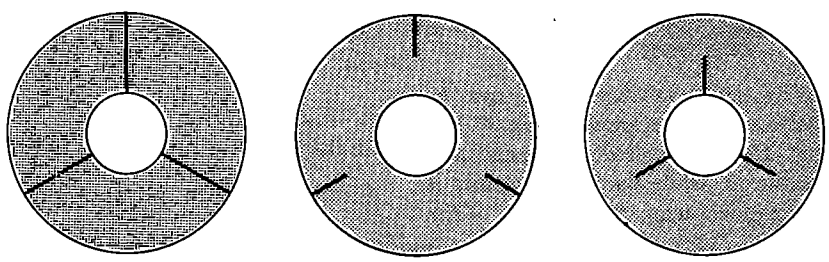

FIG. 1. A horizontal porous annulus with radial baffles, (a) full baffles, (b) inner baffles, (c) outer baffles.

$$x_0^2\frac{\partial^2\psi}{\partial x^2}+y_0^2\frac{\partial^2\psi}{\partial y^2}=-Ra(R_i R_o)^{1/2}\left(\frac{R_o}{R_i}\right)^x \times\left[x_0\frac{\partial\Theta}{\partial x}\cos\left(\frac{y}{y_0}+\theta_m\right)-y_0\frac{\partial\Theta}{\partial y}\sin\left(\frac{y}{y_0}+\theta_m\right)\right] \quad (9)$$

$$\frac{\partial\Theta}{\partial\tau}=\frac{(R_i/R_o)^{2x}}{R_i R_o}\left[x_0^2\frac{\partial^2\Theta}{\partial x^2}+y_0^2\frac{\partial^2\Theta}{\partial y^2} -x_0y_0\left(\frac{\partial\psi}{\partial y}\frac{\partial\Theta}{\partial x}-\frac{\partial\psi}{\partial x}\frac{\partial\Theta}{\partial y}\right)\right] \quad (10)$$

where $x_0 = 1/\ln(R_o/R_i)$, $y_0 = 1/(2\pi)$, $\theta_o = \pi$, $\theta_i = -\pi$ and $\theta_m = (\theta_o+\theta_i)/2$.

The transformed governing equations and boundary conditions are solved numerically by employing a finite difference method which has been successfully used by the author. The details of the numerical scheme are omitted here for brevity and may be found in refs. [2, 7, 8]. Uniform grids, 51×81, in the transformed domain, are used for the present study. It should be noted that further grid refinement did not produce any significant improvement in the calculated Nusselt numbers. As an additional check on the accuracy of the computational results, an overall energy balance has been performed after each calculation. For the present study, the energy balance is satisfied within 3%. To validate the numerical code, the solutions thus obtained have been compared with those reported in the literature for the case of a simple annulus. The agreement is very good as indicated in Fig. 2.

In view of the parameters and the complexity involved in this problem, we have restricted the geometry to the case of $r_i = 1$ and $D = 2$. For partial baffles, we have limited their length to $H = D/2$. To simplify the problem, we have further assumed that the thermal conductivity of baffles is the same as that of the porous medium. Since the purpose of using radial baffles is to reduce heat loss, it is not likely to select a baffle which has a thermal conductivity greater than that of the porous medium. Otherwise, the conduction heat loss along the baffles may outweigh the convection loss. Therefore, under this assumption, the results thus obtained can be treated as an upper bound for the problem.

For the present study, computations always start from a static condition, assuming the fluid is at rest in the beginning of simulation. Previous solutions were not used as the starting condition for the subsequent calculations. The computational results have covered a range of Rayleigh numbers of practical interest (i.e. $50 \leqslant Ra \leqslant 500$). For a given Rayleigh number, calculations have been performed to obtain results for a complete set of baffle orientations.

NUMERICAL RESULTS AND DISCUSSION

The flow and temperature fields for an annulus with 3 full baffles are first shown in Figs. 3(a) and (b), respectively. The corresponding fields for an annulus with no baffle are also included for comparison. To reveal the changes of flow and isotherm patterns with the orientation of baffles, the referenced baffle has been specially marked. Also, for the convenience of discussion that follows, the sectors have been numbered as indicated in Fig. 3(a). Since the geometry repeats

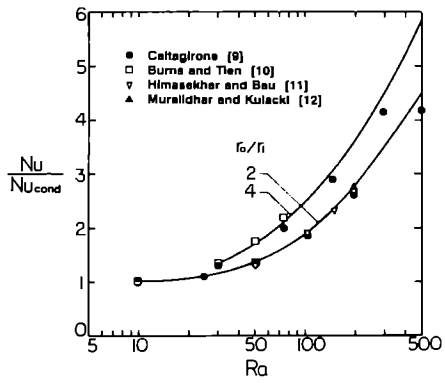

FIG. 2. A comparison of the results obtained from the present study and those reported in the literature for a simple annulus.

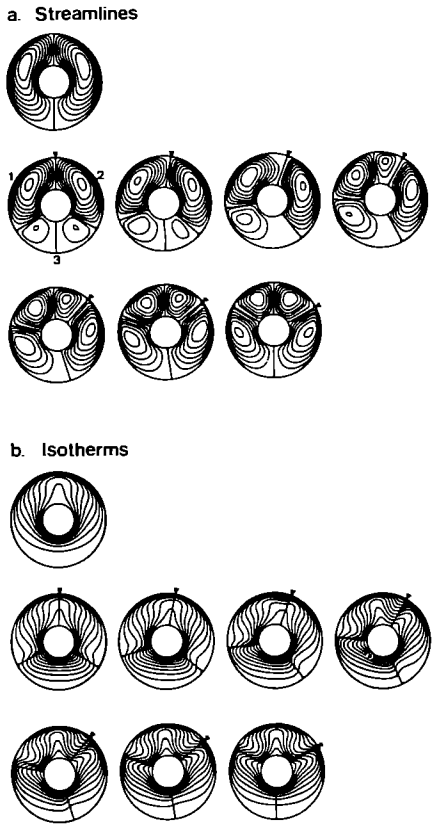

FIG. 3. Flow and temperature fields for an annulus with 3 full baffles ($Ra = 100$, $\Delta\psi = 1$ and $\Delta\Theta = 0.1$).

itself for every 120° of rotation, the variation of flow and isotherm patterns will also have a periodicity of 120°.

For a simple annulus, natural convection is established in the form of two primary cells. However, when radial baffles are inserted to the annulus, these two primary cells are confined to a smaller region. In addition, a second pair of recirculating cells is formed in the lower region of the annulus. When the annulus is rotated 10° from its initial position, the strength of the two primary cells is slightly decreased. But, more obvious is the change in the strength of secondary cells. At $\gamma = 20°$, the strength of the primary cells continues to decrease. On the other hand, the flow structure in sector 3 has changed from a bicellular flow to a unicellular flow. At $\gamma = 30°$, a secondary flow is formed in sector 1. As the orientation angle increases, the secondary flow continues to grow while the primary cells are weakening. Due to the symmetry at $\gamma = 60°$, not only do the two cells in sector 1 have equal strength, but also the cell in sectors 2 and 3 has the same strength. If the annulus is rotated further, it is found that the flow pattern at $\gamma = 70°$ is a mirror reflection of that at 50°. Similarly, the flow pattern at 80° is a reflection of that at 40°. For brevity, only the flow and temperature fields for $\gamma \leqslant 60°$ are displayed here.

For a simple annulus, the temperature gradient at the lower half of the inner cylinder is very large due to convection (Fig. 3(b)). However, for a partitioned annulus, the convective flow is blocked by the radial baffles. The heat transfer in the lower sector is mainly by conduction. In comparison to that for a simple annulus, the temperature gradient is relatively small. As the annulus is rotated through 30°, a reversed thermal plume is found in sector 1. This reversed plume is the cause for the secondary flow that was observed in the flow pattern. As a result, the temperature gradient at the upper half of the inner cylinder is increased. It is also interesting to note that the heat transfer mode in sector 3 has changed gradually from conduction to convection as the orientation angle increases.

For an annulus with 3 outer baffles, the flow and temperature fields are shown in Figs. 4(a) and (b), respectively. The flow field of this case looks very similar to that of the previous case. The similarity is that, for both cases, a secondary flow is formed in sector 1 when the orientation angle increases. In fact, for outer baffles, the secondary flow appears earlier at $\gamma = 20°$ instead of 30° for the full baffles. However, there also exists a major difference between these two cases. The difference is due to the blockage of convective flow. For outer baffles, the convective flow is only partially blocked such that the heat transfer in sector 3 is primarily by convection. Since the secondary flow in this case never separates from the primary cell, the temperature gradient on the upper inner cylinder is small in comparison to that for the case of full baffles.

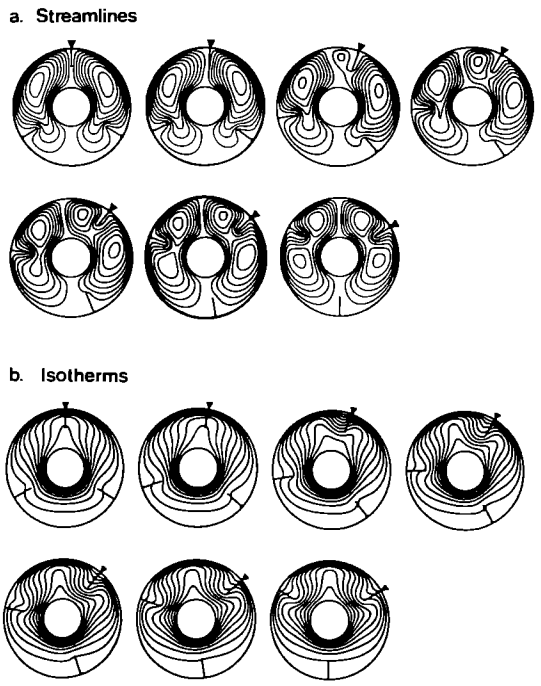

FIG. 4. Flow and temperature fields for an annulus with 3 outer baffles ($Ra = 100$, $\Delta\psi = 1$ and $\Delta\Theta = 0.1$).

The flow and temperature fields for an annulus with 3 inner baffles are shown in Figs. 5(a) and (b), respectively. Since there is no formation of a secondary flow, the flow patterns of this case are very

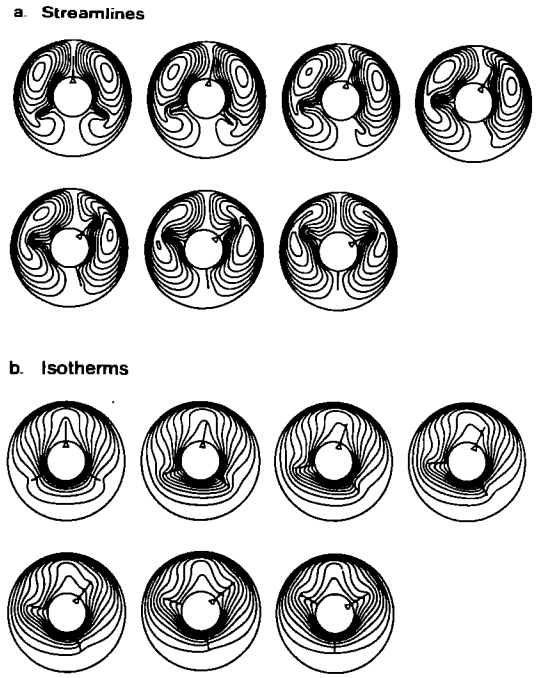

FIG. 5. Flow and temperature fields for an annulus with 3 inner baffles ($Ra = 100$, $\Delta\psi = 1$ and $\Delta\Theta = 0.1$).

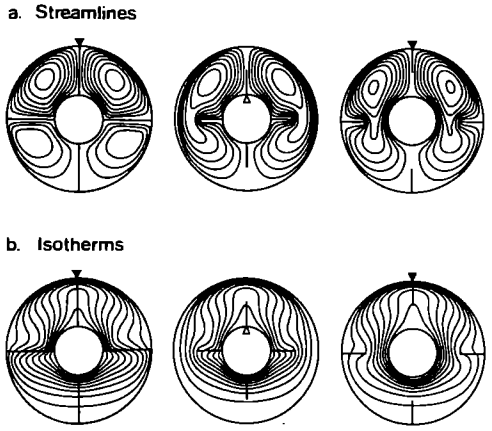

FIG. 6. Flow and temperature fields for an annulus with 4 baffles ($Ra = 100$, $\gamma = 0$, $\Delta\psi = 1$ and $\Delta\Theta = 0.1$).

different from the previous two cases. Basically, the convective flow in this case has the same form as that for a simple annulus, i.e. two primary cells. However, the strength of the recirculating cells is weaker for the present case. Since there is no secondary flow, the temperature gradient at the upper half of inner cylinder has a smallest value among the three cases examined in this study. It is important to recognize the difference in basic functions between the inner and outer baffles. While the inner baffles are used to block the heated fluid which rises to the top, the outer baffles are used to barricade the cooled fluid which returns to the bottom. Because of this fundamental difference, the heat transfer results also vary as will be discussed later.

As the number of baffles increases, the flow and temperature fields become more complicated as shown in Figs. 6 and 7. Due to the increased resistance, the strength of convective flow has been considerably weakened. As a result, the temperature gradient on the inner cylinder is also reduced. Although not shown explicitly, it is clear that, for an annulus with 4 baffles, the variation of the flow and isotherm patterns will repeat itself for every 90° of rotation. Similarly, it is 60° for an annulus with 6 baffles.

At a high Rayleigh number ($Ra = 500$), the flow and temperature fields at some orientation angles did not converge. For these cases, a transient analysis was performed to investigate the origin of instability. The transient analysis employed here is essentially the same as that reported in ref. [13]. Therefore, the details of the analysis are omitted here for brevity. However, it should be mentioned that the flow and temperature fields for the present case are inherently more unstable such that a smaller time step is required ($\Delta\tau = 10^{-5}$ is used for the present study).

The variation of flow field with time is shown in Fig. 8 for an annulus with 3 full baffles. It should be mentioned, however, that the variation of flow field for other cases, although not shown here, is qualitatively the same. It is interesting to observe that the flow instability is primarily localized on sector 1. The flow in the other two sectors is basically independent of time. The oscillatory flow observed here is very similar to that in a rectangular enclosure [14]. For the latter, Horne and O'Sullivan [14] have concluded that the flow oscillation is a result of combined influence of cyclic triggering by predecessor disturbance which circulate around the region and instability in the thermal boundary layer on the heated surface. More recently, Kimura *et al.* [15] have reported that thermal convection at high Rayleigh numbers may either lead to a steady multicellular flow or undergo a transition from steady state to time-dependent flow. Similar conclusions have also been reported for a horizontal porous annulus [16]. Qualitatively, these conclusions can also apply to the present case.

The result of primary interest in this study is the heat transfer coefficient. The heat transfer coefficient in terms of the Nussult number is given by

$$Nu = \frac{hD}{k} = -\frac{1}{R_i \ln (R_o/R_i)} \int_{-1/2}^{1/2} \left.\frac{\partial\Theta}{\partial x}\right|_{x=-1/2} \mathrm{d}y. \tag{11}$$

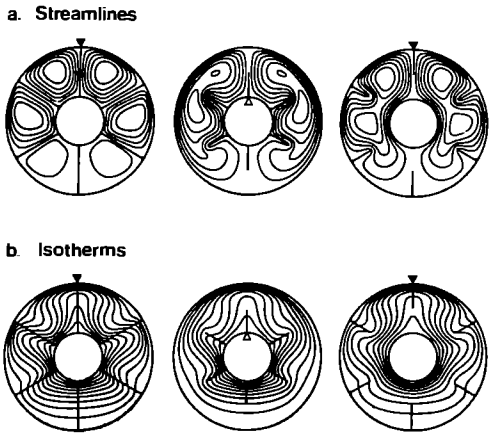

FIG. 7. Flow and temperature fields for an annulus with 6 baffles ($Ra = 100$, $\gamma = 0°$, $\Delta\psi = 1$ and $\Delta\Theta = 0.1$).

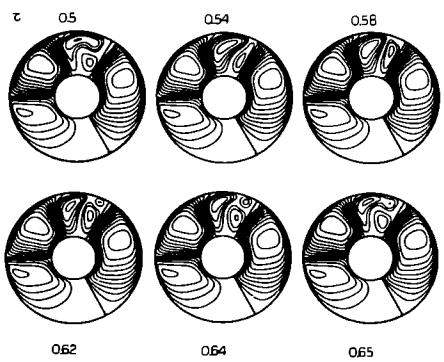

FIG. 8. Oscillatory flow fields for an annulus with 3 full baffles at $\gamma = 30°$ ($\Delta\psi = 2$).

However, heat transfer results for the problem under consideration are most informative if the Nusselt number thus obtained is normalized by the conduction value. In this case, the normalized Nusselt number also shows the relative importance of convection to conduction. It is easy to show that the conduction Nusselt number can be evaluated as,

$$Nu_{\text{cond}} = \frac{1}{R_i \ln (R_o/R_i)}. \tag{12}$$

The normalized Nusselt numbers for $N = 3$ are plotted in Fig. 9 as a function of the Rayleigh number and baffle orientation angle. First, it is clearly observed that radial baffles are very effective in reducing heat losses from pipe insulation. In addition, partial baffles are generally more effective than full baffles. For example, at $Ra = 100$, the maximum reduction of heat loss is 8% for full baffles and is 10% for inner baffles. Secondly, for $Ra \geqslant 100$, the variation of normalized Nusselt numbers seems to have two distinct characteristics for the cases of full and outer baffles. As observed earlier, a secondary flow is formed in the annulus for these two cases as the orientation angle increases. For example, when $Ra = 100$, the secondary flow is formed at $\gamma = 30$ for the case of full baffles and at $\gamma = 20$ for outer baffles. Therefore, one can conclude that the first characteristic is associated with the processes before the secondary flow is generated and the second characteristic is related to the processes afterwards.

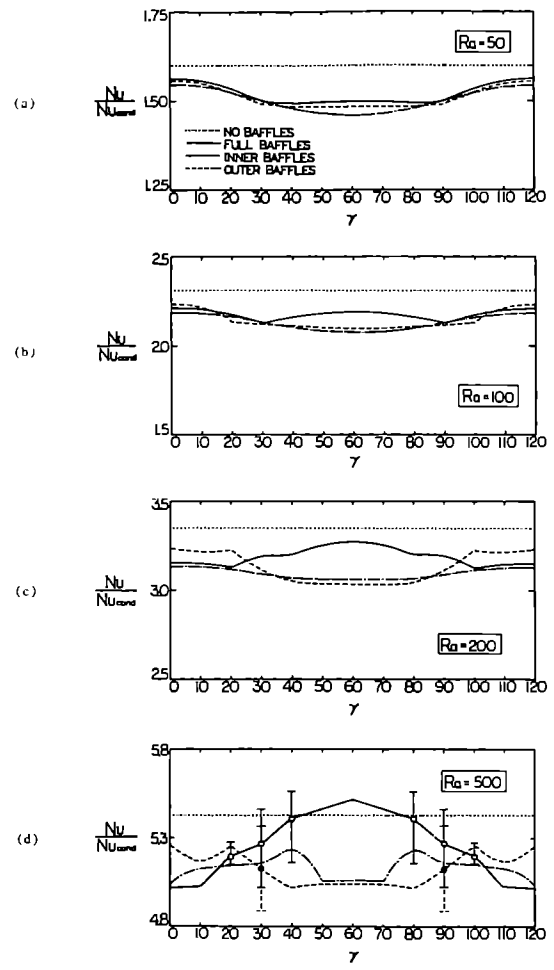

FIG. 9. Normalized Nusselt numbers for an annulus with 3 baffles at various orientation angles.

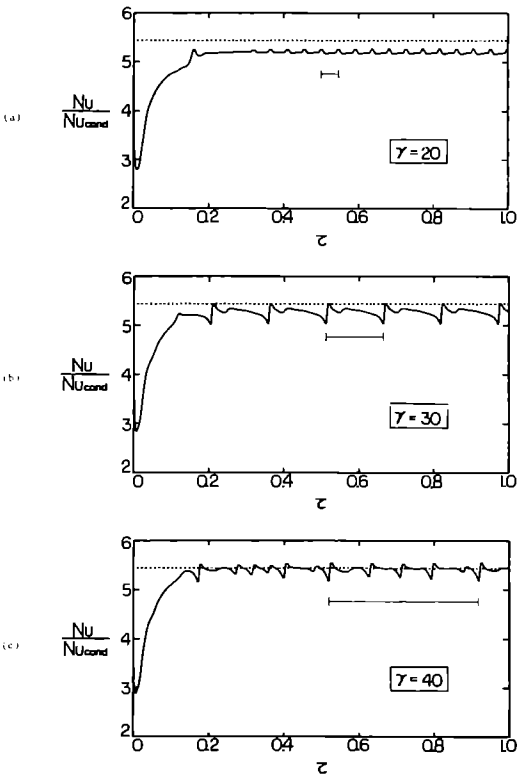

FIG. 10. Variations of normalized Nusselt numbers with time for an annulus with 3 full baffles, (a) $\gamma = 20$, (b) $\gamma = 30$ and (c) $\gamma = 40$.

As observed earlier, when $Ra = 500$, the flow and temperature fields for baffles at certain orientation angles become oscillating. For these cases, the averaged Nusselt numbers and their extreme values are also plotted in the figure. The variation of Nusselt numbers with time is shown in Fig. 10 for an annulus with 3 full baffles. The line segment shown in the figure represents a period of oscillation. It is clear that the period of oscillation increases with the orientation angle. In addition, it is observed that the periodic pattern becomes more complicated as the orientation angle increases.

For completeness, the normalized Nusselt numbers for $N = 4$ and 6 are shown in Figs. 11 and 12, respectively. Clearly, the effectiveness of pipe insulation has greatly improved as more baffles are utilized. For $N = 4$, the maximum reduction in heat loss at $Ra = 100$ is 12% for the full baffles and it is increased to 18% when $N = 6$. Similarly, for partial baffles, it has increased from 12% for $N = 4$ to 19% when $N = 6$.

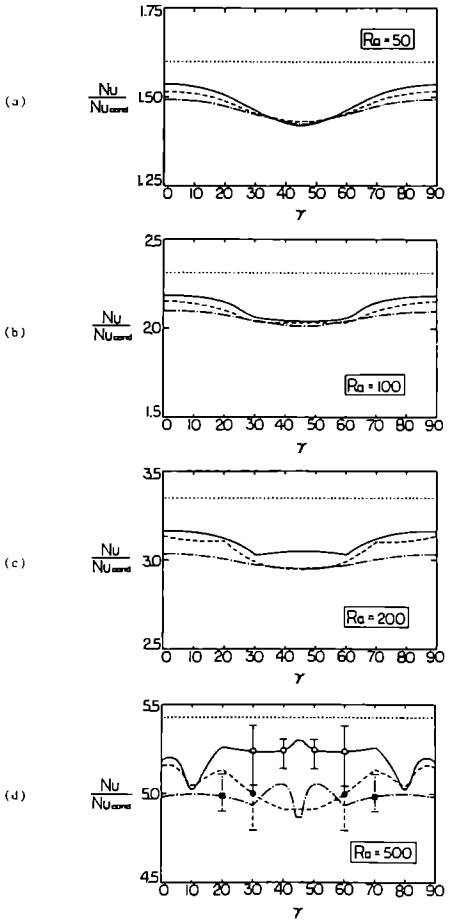

FIG. 11. Normalized Nusselt numbers for an annulus with 4 baffles at various orientation angles.

For practical applications, it is important to adjust the baffle orientation in order to maximize the effectiveness. Table 1 is provided as a summary of the optimal baffle configurations determined by this study.

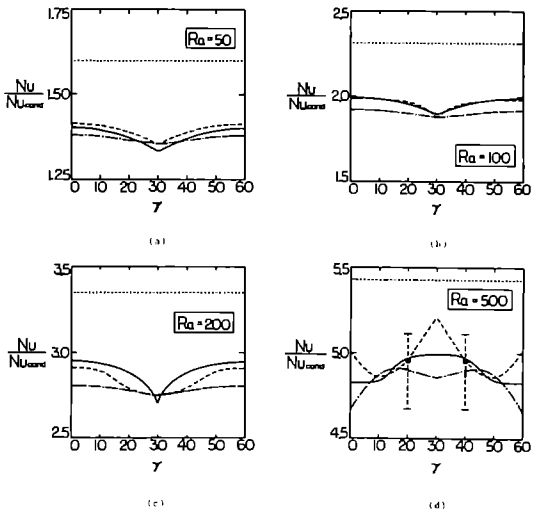

FIG. 12. Normalized Nusselt numbers for an annulus with 6 baffles at various orientation angles.

CONCLUSION

Numerical results have been presented for natural convection in a horizontal porous annulus with radial baffles. The results thus obtained have some interesting implications for the design of pipe insulation:

(1) Radial baffles prove to be effective in reducing heat losses from a pipe insulation. The effectiveness increases with the baffle number.

(2) In general, partial baffles are more effective than full baffles. Between two partial baffles, inner baffles work better than outer baffles.

(3) For a given set of pipe insulation, it is important to adjust the baffle orientation so as to maximize the effectiveness.

(4) At high Rayleigh numbers, the flow and temperature fields become unstable. The averaged heat transfer, however, is still less when using baffles.

Table 1. Optimum orientation angle for a maximum reduction in heat loss from a horizontal pipe insulation

	Ra			
Baffle geometry	50	100	200	500
$N = 3$				
Full baffles	40 (6%)†	30 (8%)	20 (7%)	0 (7%)
Outer baffles	60 (7%)	60 (9%)	60 (9%)	40 (7%)
Inner baffles	60 (9%)	60 (10%)	60 (9%)	0 (7%)
$N = 4$				
Full baffles	45 (11%)	45 (12%)	30 (9%)	10 (7%)
Outer baffles	45 (10%)	30 (12%)	45 (12%)	40 (9%)
Inner baffles	45 (11%)	45 (13%)	45 (12%)	45 (10%)
$N = 6$				
Full baffles	30 (16%)	30 (18%)	30 (19%)	0 (10%)
Outer baffles	30 (15%)	30 (18%)	30 (18%)	10 (10%)
Inner baffles	30 (15%)	30 (19%)	30 (18%)	10 (10%)

†Numbers in parentheses designate the maximum reduction in heat loss.

Acknowledgements—The author is grateful for the valuable suggestions of the reviewers. The support of this work by the Academic Computing and Networking Services at the Colorado State University is also gratefully acknowledged.

REFERENCES

1. H. H. Bau, Low Rayleigh number thermal convection in a saturated porous medium bounded by two eccentric cylinders, *J. Heat Transfer* **106,** 166–175 (1984).
2. F. C. Lai and F. A. Kulacki, Natural convection across a vertical layered porous cavity, *Int. J. Heat Mass Transfer* **31,** 1247–1260 (1988).
3. M. J. Shilston and S. D. Probert, Effects of horizontal and vertical spacers on the heat transfer across a horizontal, annular, air-filled cavity, *Appl. Energy* **4,** 21–37 (1978).
4. S. S. Kwon, T. H. Kuehn and T. S. Lee, Natural convection in the annulus between horizontal circular cylinders with three axial spacers, *J. Heat Transfer* **104,** 118–124 (1982).
5. R. F. Babus'Haq, S. D. Probert and M. J. Shilston, Influence of baffles upon natural-convective steady-state heat transfer across horizontal air-filled annuli, *Proc. 8th Int. Heat Transfer Conf.*, Vol. 4, pp. 1557–1561 (1986).
6. S. V. Patankar and J. C. Chai, Laminar natural convection in internally finned horizontal annuli, ASME Paper 91-HT-12 (1991).
7. I. Pop and F. C. Lai, Natural convection in a truncated circular sector of porous medium, *Int. Commun. Heat Mass Transfer* **17,** 801–811 (1990).
8. F. C. Lai, V. Prasad and F. A. Kulacki, Aiding and opposing mixed convection in a vertical porous layer with a finite wall heat source, *Int. J. Heat Mass Transfer* **31,** 1049–1061 (1988).
9. J. P. Caltagirone, Thermoconvective instabilities in a porous medium bounded by two concentric horizontal cylinders, *J. Fluid Mech.* **76,** 337–362 (1976).
10. P. J. Burns and C. L. Tien, Natural convection in porous media bounded by concentric spheres and horizontal cylinders, *Int. J. Heat Mass Transfer* **22,** 929–939 (1979).
11. K. Himasekhar and H. H. Bau, Large Rayleigh number convection in a horizontal, eccentric annulus containing saturated porous media, *Int. J. Heat Mass Transfer* **29,** 703–712 (1986).
12. K. Muralidhar and F. A. Kulacki, Non-Darcy natural convection in a saturated horizontal porous annulus, *J. Heat Transfer* **110,** 133–139 (1988).
13. F. C. Lai and F. A. Kulacki, Oscillatory mixed convection in horizontal porous layers locally heated from below, *Int. J. Heat Mass Transfer* **34,** 887–890 (1991).
14. R. N. Horne and M. J. O'Sullivan, Oscillatory convection in a porous medium heated from below, *J. Fluid Mech.* **66,** 339–352 (1974).
15. S. Kimura, G. Schubert and J. M. Straus, Route to chaos in porous medium convection, *J. Fluid Mech.* **166,** 305–324 (1986).
16. Y. F. Rao, K. Fukuda and S. Hasegawa, Steady and transient analyses of natural convection in a horizontal porous annulus with the Galerkin method, *J. Heat Transfer* **109,** 919–927 (1987).